ARTICLE IN PRESS

Available online at www.sciencedirect.com

SCIENCE DIRECT®

Computers and Chemical Engineering xxx (2003) xxx–xxx

Computers & Chemical Engineering

www.elsevier.com/locate/compchemeng

A novel partial differential algebraic equation (PDAE) solver: iterative space–time conservation element/solution element (CE/SE) method

Young-Il Lim [a,*], Sin-Chung Chang [b], Sten Bay Jørgensen [a]

[a] *Computer-Aided Process Engineering Center (CAPEC), Department of Chemical Engineering, Technical University of Denmark, 2800 Kgs. Lyngby, Denmark*

[b] *MS 5-11, NASA Glenn Research Center, 21000 Brookpark Road, Cleveland, OH 44135, USA*

Received 16 April 2003; received in revised form 3 September 2003; accepted 3 September 2003

Abstract

For solving partial differential algebraic equations (PDAEs), the space–time conservation element/solution element (CE/SE) method is addressed in this study. The method of lines (MOL) using an implicit time integrator is compared with the CE/SE method in terms of computational efficiency, solution accuracy and stability. The space–time CE/SE method is successfully implemented to solve PDAE systems through combining an iteration procedure for nonlinear algebraic equations. For illustration, chromatographic adsorption problems including convection, diffusion and reaction terms with a linear or nonlinear adsorption isotherm are solved by the two methods.

The CE/SE method enforces both local and global flux conservation in space and time, and uses a simple stencil structure (two points at the previous time level and one point at the present time level). Thus, accurate and computationally-efficient numerical solutions are obtained. Stable solutions are guaranteed if the Courant–Friedrichs–Lewy (CFL) condition is satisfied. Solutions to two case studies demonstrate that the CE/SE numerical solutions are comparative in accuracy to those obtained from a MOL discretized by the 5th-order weighted essentially non-oscillatory (WENO) upwinding scheme with a significantly shorter calculation time.

Keywords: Numerical analysis; Partial differential algebraic equations (PDAEs); Space–time CE/SE method; Method of lines (MOL); Chromatographic adsorption problem; Protein ion-exchange separation

1. Introduction

In selecting a numerical method for solving a system of partial differential equations (PDEs), one often needs to make some compromises in the method's accuracy, efficiency and robustness. As an example, for the sake of higher efficiency and robustness, often one is forced to choose a solver with less accuracy. However, as will be shown in the following study which involves the method of lines (MOL) and the space–time conservation element and solution element (CE/SE) method, in some rare cases, such a forced compromise may not be necessary.

In the framework of the method of lines (MOL), PDEs or PDAEs are converted to an ordinary differential equation (ODE) or differential algebraic equation (DAE) system in the temporal space after spatial discretization. The ODE (or DAE) time integrator (e.g. Gear-type algorithms) gives high accuracy solutions with respect to time through adjusting the time step-size (Δt) adaptively to the stiffness of the ODE/DAE system considered. For the numerical solution of practical chemical processes, Lim, Le Lann, and Joulia (2001a) and Lim et al. (2002) have implemented high resolution upwinding schemes (e.g. WENO scheme, Jiang & Shu, 1996) within the framework of the MOL. However, numerical dissipation caused by spatial discretization can still be substantial in the presence of steep fronts when the number of mesh points is insufficient. To capture the steep front, moving mesh methods using the MOL were examined. However, such approaches generally require long computational times because of strong coupling and non-linearity between original physical PDEs and mesh equations added for mesh calculation (Lim, Le Lann, & Joulia, 2001b).

Many physical problems are modeled with Partial Differential Algebraic Equation (PDAE) systems. For example, the packed-bed chromatographic separation can be described by convection-dominated parabolic Partial Differential Equations (PDEs) for mass conservation in the mobile phase,

* Corresponding author. Tel.: +45-4525-2802; fax: +45-4593-2906.
E-mail address: lim@kt.dtu.dk (Y.-I. Lim).

0098-1354/$ – see front matter © 2003 Elsevier Ltd. All rights reserved.
doi:10.1016/j.compchemeng.2003.09.016

Nomenclature

a_i	activity in the liquid phase (mol/l)
$\bar{a}_i$	activity in the solid phase (mol/l)
B	Debye–Hückel model parameter (kg/mol)
C_i	concentration in fluid phase (mol/l)
C_{in}	entrance concentration of fluid at $z = 0$ (mol/l)
C_{out}	exit concentration of fluid at $z = z_{\text{f}}$ (mol/l)
D_{ax}	axial dispersion coefficient (m^2/s)
E_2	two-dimensional Euclidean spaces
$\tilde{F}_j^n$	approximated conservation fluxes in CE(j, n)
f	fluxes
f_t	$\partial f/\partial t$
f_u	$\partial f/\partial u$
f_z	$\partial f/\partial z$
g	adsorption isotherm function in Eq. (1)
h	vector, $h = (f, u)$
I	ionic strength (mol/kg-solvent)
j	subscript for mesh positions
J	number of non-zero Jacobian elements
k	effective adsorption rate coefficient (s^{-1})
K_{ji}	equilibrium constant between i–j components
L_{c}	column length (m)
m	adsorption heat (kcal/mol)
m_i	molarity (mol/kg-solvent)
M_{w}	molecular weight (g/mol)
n	superscript for time levels
$\boldsymbol{n}$	outward normal vector of a surface element on $S(V)$
n_i^*	equilibrium concentration in interface between two phases (mol/l)
n_i	concentration in solid phase (mol/l)
$\hat{n}_i$	hindered salt ion concentration (mol/l)
n_{T}	resin capacity (eq./l)
N_{mesh}	number of mesh points
N_{time}	number of time steps
p	source terms
$\tilde{P}_j^n$	approximated source term fluxes in CE(n, j)
R	gas constant (kcal/(K mol))
s	values obtained at previous time level in Eq. (10)
S_i	shape factor
$S(V)$	boundary of an arbitrary space–time region V
t	time (s)
Δt	uniform time step size (s)
T	temperature (K)
u	state variables
u_t	$\partial u/\partial t$
u_z	$\partial u/\partial z$
v_{L}	fluid velocity (m/s)
V	space–time region in E_2
y_i	molar fraction of equilibrium concentrations
z	axial direction of column (m)
z_i	ion valence
$z_\pm$	positive or negative charge of salt
Δz	uniform spatial step size (m)

Greek letters

α	phase ratio of solid volume to fluid volume (kg/l-resin)
α_{ij}	Boltzmann weighting factor
ε_{b}	bed voidage
γ_i	activity coefficient in the liquid phase
$\bar{\gamma}_i$	activity coefficient in the solid phase
ν	CFL number
ρ_{r}	wet resin density (kg/l-resin)
σ	area of a surface element on $S(V)$ or steric factor (or hindered-salt ion ratio)
ω_i	surface fraction

Ordinary Differential Equations (ODEs) for the solute adsorption rate in the stationary phase, and eventually Algebraic Equations (AEs) for the adsorption isotherm between the two phases. Thus, they lead to a nonlinear and coupled PDAE system which is often solved, after discretization of spatial derivatives, by ODE/Differential Algebraic Equation (DAE) time-integrators in the framework of the MOL (Beste, Lisso, Wozny, & Arlt, 2000; Dunnebier, Weirich, & Klatt, 1998; Ma & Wang, 1997; Melis, Markos, Cao, & Morbidelli, 1996). However, the solution procedure may be inadequate for multi-component and -dimensional systems since the DAE system obtained from spatial discretization of the PDAEs can be steep in the axial direction, large in the Jacobian matrix size, nonlinear between state variables, iterative in the solution procedure or numerically-dissipative. Therefore, a new numerical method, such as the one presented here, is needed to enhance accuracy and computational efficiency.

For the numerical solution of conservation laws (e.g. PDEs), Chang and To (1991) proposed a new method, the so-called space–time Conservation Element and Solution Element or the CE/SE method for short, which is accurate even at discontinuities and is computationally efficient. By using the Gauss's divergence theorem, the CE/SE method enforces both local and global flux conservation in space and time. Also because each CE/SE scheme is developed from a non-dissipative core scheme, its numerical dissipation can be effectively controlled. While the MOL with a stiff DAE time integrator (e.g. DASSL, Petzold, 1983; SPRINT, Pennington & Berzins, 1993; LSODI, Hindmarsch, 1980) has an implicit feature with variable time steps and requires much computational time on fine meshes, the CE/SE method is an explicit time-marching scheme with a simple stencil structure (two points at the previous time level and one point at the present time level) and, as such, is more computationally efficient. Rather than a compromise

between accuracy and computational efficiency in the numerical method selection, higher accuracy as well as efficiency can, consequently, be achieved by the novel method.

In spite of the fact that the schemes constructed using the space–time CE/SE method generally are 2nd-order or less in accuracy (Chang & To, 1991; Chang, Wang, & To, 2000), the new method has been used to obtain highly accurate numerical solutions for 1D, 2D, and 3D conservation laws involving shocks, boundary layers or contacting discontinuities (Chang, 1995; Chang, Wang, & Chow, 1999). The Courant number insensitive Scheme II (Chang, 2002) has recently been proposed for the Euler equations (e.g. convection PDEs for mass, momentum and energy conservation). The a–μ scheme (Chang, 1995) has been developed for the Navier–Stokes equations (e.g. convection–diffusion PDEs for mass, momentum and energy conservation). An implicit solver for boundary value problems (Chang, Wang, Chow, & Himansu, 1995), multi-dimensional CE/SE (Chang et al., 1999; Zhang et al., 2002), local mesh refinement (Chang, Wu, Wang, & Yang, 2000) and stiff source term treatment for convection-reaction PDEs (Yu & Chang, 1997) have been presented for the space–time CE/SE method. For any reader who is interested in the CE/SE simulation, the Fortran code is available in Chang (1995, 2002).

Molls and Molls (1998) used the CE/SE method to solve the 1D/2D Saint Venant equations. Here, a modified CE/SE method (i.e. non-iterative formulae) was proposed for solving PDEs including source terms (or reaction terms). Motz, Mitrovic, and Gilles (2002) successfully applied this method to solve a population balance equation described by a hyperbolic integro-PDE, where superior numerical performance of the CE/SE method is shown over a method of lines with a flux-limited finite volume scheme.

Finally note that, in addition to the MOL and the CE/SE method discussed here, there are other reputable methods which could be used to solve the same sample problems to be presented in this study. A good source of references in this respect is the paper by Poulain and Finlayson (1993). Moreover, numerical comparisons of the CE/SE method and other established methods (e.g. MacCormack method) can also be found in Chang et al. (2000).

The present study addresses an extension of the CE/SE method of Chang (2002) to PDAE systems. In the next section, the CE/SE method is reformulated for PDAE systems, illustrating the packed-bed chromatographic separation problem. Numerical studies follow in Section 3.

2. Space–time CE/SE method

The CE/SE method has many non-traditional features, including a unified treatment of space and time, the introduction of conservation element (CE) and solution element (SE) and a novel shock capturing strategy without special techniques.

Consider a packed-bed chromatographic adsorption between the stationary and mobile phases. The PDAE system involves one PDE, one ODE and one AE:

$$\frac{\partial C}{\partial t} + \alpha\frac{\mathrm{d}n}{\mathrm{d}t} + \frac{\partial(v_{\mathrm{L}}C)}{\partial z} - \frac{\partial}{\partial z}\left(D_{\mathrm{ax}}\frac{\partial C}{\partial z}\right) = 0 \tag{1a}$$

$$\frac{\mathrm{d}n}{\mathrm{d}t} = k(n^* - n) \tag{1b}$$

$$0 = g(C, n^*) \tag{1c}$$

where v_{L} is the interstitial velocity, D_{ax} the axial dispersion coefficient, α the volume ratio between the two phases and k refers to the mass transfer coefficient. The liquid and solid concentrations for each component are referred to as C and n, respectively. n^* is the equilibrium concentration (or adsorption isotherm). C and n^* is related by the functional relation Eq. (1c) whose exact form used in the numerical simulations is case-dependent. Since the Peclet number for axial diffusion (ratio of convection to diffusion, $Pe = v_{\mathrm{L}}L_{\mathrm{c}}/D_{\mathrm{ax}}$) is often large in chromatographic processes (Poulain & Finlayson, 1993), Eq. (1) is classified as a convection-dominated parabolic PDAE system. The extension to the PDAE system is derived from the original CE/SE method (Chang, 1995) and Scheme II (Chang, 2002), introducing CEs and SEs.

2.1. Conservation elements (CEs) and solution elements (SEs)

As a preliminary, let state variables (u), fluxes (f) and source terms (p) in Eq. (1):

$$u = \begin{pmatrix} u_1 \\ u_2 \\ u_3 \end{pmatrix} \equiv \begin{pmatrix} C + \alpha n \\ n \\ 0 \end{pmatrix} \tag{2a}$$

$$f = \begin{pmatrix} f_1 \\ f_2 \\ f_3 \end{pmatrix} \equiv \begin{pmatrix} v_{\mathrm{L}}C - D_{\mathrm{ax}}\dfrac{\partial C}{\partial z} \\ 0 \\ 0 \end{pmatrix} \tag{2b}$$

$$p = \begin{pmatrix} p_1 \\ p_2 \\ p_3 \end{pmatrix} \equiv \begin{pmatrix} 0 \\ k(n^* - n) \\ g(C, n^*) \end{pmatrix} \tag{2c}$$

Let (i) $h_m =^{\mathrm{def}} (f_m, u_m)$, $m = 1$–3; (ii) $\nabla =^{\mathrm{def}} (\partial/\partial z, \partial/\partial t)$, i.e. ∇ is the divergence operator in a two-dimensional Euclidian space E_2 in which $x_1 = z$ and $x_2 = t$ are the space and time coordinates. Then the three component equations referred to above can be expressed as:

$$\nabla \cdot h_m = p_m, \quad m = 1\text{–}3 \tag{3}$$

By using Gauss's divergence theorem in E_2, it can be shown that Eq. (3) is the differential form of the integral conservation law:

$$\oint_{S(V)} h_m \,\mathrm{d}s = \int_V p_m \,\mathrm{d}V, \quad m = 1\text{–}3 \tag{4}$$

where (i) $S(V)$ is the boundary of an arbitrary space–time region V in E_2; (ii) $\mathrm{d}s = \mathrm{d}\sigma \boldsymbol{n}$ with $\mathrm{d}\sigma$ and $\boldsymbol{n}$, respectively, being the area and the outward normal vector of a surface element on $S(V)$. Note that, because $h_m\,\mathrm{d}s$ is the space–time flux of h_m leaving the region V through the surface element ds, Eq. (4) simply states that, for each $m = 1$–3, the total space–time flux of h_m leaving V through $S(V)$ is equal to the integral of p_m over V. Also, since, in E_2, $\mathrm{d}\sigma$ is the length of a differential line segment on the simple closed curve $S(V)$, the surface integral on the left side of Eq. (4) can be converted into a line integral. In fact, Eq. (4) is equivalent to (Chang, 1995):

$$\oint_{S(V)}^{\text{c.c.}} (-u_m\,\mathrm{d}z + f_m\,\mathrm{d}t) = \int_V p_m\,\mathrm{d}V, \quad m = 1\text{–}3 \tag{5}$$

where the notation c.c. indicates that the line integral should be carried out in the counterclockwise direction.

At this junction, note that the CE/SE method is developed to model space–time conservation laws such as those represented by Eq. (4). As will be shown shortly, its nontraditional features include: (i) a unified treatment of space–time; (ii) the introduction of conservation elements (CEs) and solution elements (SEs) as the vehicles for enforcing conservation laws; (iii) the requirement that a numerical scheme be built from a non-dissipative core scheme such that the numerical dissipation can be effectively controlled; (iv) the requirement that the mesh values of the state variables (u_m) and their spatial derivatives ($\partial u_m/\partial z$) be considered as independent marching variables to be solved for simultaneously; and (v) a time marching strategy that has a space–time staggered stencil at its core and, as such, can capture shocks without using Riemann Solvers.

In Fig. 1, the mesh points (e.g. points A, C and E) are marked by circles. They are staggered in space–time. Any mesh point (j, n) is associated with a solution element SE(j, n) and two conservation elements CE$_-(j, n)$ and CE$_+(j, n)$. By definition, SE(j, n) is the interior of the shaded space–time region depicted in Fig. 1(a). It includes a horizontal line segment, a vertical line segment, and their immediate neighborhood (Chang, 1995). Also, by definition, (i) CE$_-(j, n)$ and CE$_+(j, n)$, respectively, are the rectangles ABCD and ADEF depicted in Fig. 1(a) and (b); and (ii) CE(j, n) is the union of CE$_-(j, n)$ and CE$_+(j, n)$, i.e. the rectangle BCEF.

Let the coordinate of any mesh point (j, n) be (z_j, t^n) with $z_j = j\,\Delta z$ and $t^n = t\,\Delta z$. Then, for any $(z, t) \in$ SE(j, n), $u_m(z, t)$, $f_m(z, t)$ and $h_m(z, t)$, respectively, are approximated by a 1st-order Taylor expansion:

$$\tilde{u}_m(z, t; j, n) \overset{\text{def}}{=} (u_m)_j^n + (u_{mz})_j^n (z - z_j) + (u_{mt})_j^n (t - t^n), \quad m = 1\text{–}3 \tag{6}$$

$$\tilde{f}_m(z, t; j, n) \overset{\text{def}}{=} (f_m)_j^n + (f_{mz})_j^n (z - z_j) + (f_{mt})_j^n (t - t^n), \quad m = 1\text{–}3 \tag{7}$$

and

$$\tilde{h}_m(z, t; j, n) \overset{\text{def}}{=} (\tilde{f}_m(z, t; j, n), \tilde{u}_m(z, t; j, n)), \quad m = 1\text{–}3 \tag{8}$$

Here, $(u_m)_j^n$, $(u_{mz})_j^n$, $(u_{mt})_j^n$, $(f_m)_j^n$, $(f_{mz})_j^n$ and $(f_{mt})_j^n$ are constants in SE(j, n). They, respectively, can be considered as the numerical analogues of the values of u_m, $\partial u_m/\partial z$, $\partial u_m/\partial t$, f_m, $\partial f_m/\partial z$ and $\partial f_m/\partial t$ at (z_j, t^n), respectively.

Note that, according to Eqs. (2a) and (2b), $u_3 \equiv 0$, $f_2 \equiv 0$ and $f_3 \equiv 0$. As a result, it is assumed that

$$(u_3)_j^n = (u_{3z})_j^n = (u_{3t})_j^n = 0 \tag{9}$$

$$(f_2)_j^n = (f_{2z})_j^n = (f_{2t})_j^n = 0 \tag{10}$$

$$(f_3)_j^n = (f_{3z})_j^n = (f_{3t})_j^n = 0 \tag{11}$$

In the CE/SE framework, $(u_{mt})_j^n$, $(f_m)_j^n$, $(f_{mz})_j^n$ and $(f_{mt})_j^n$, $m = 1$–3, are considered as functions of $(u_m)_j^n$ and $(u_{mz})_j^n$, $m = 1$–3. As a result of Eqs. (9)–(11), this general rule implies that $(u_{1t})_j^n$, $(u_{2t})_j^n$, $(f_1)_j^n$, $(f_{1z})_j^n$ and $(f_{1t})_j^n$ must be considered as functions of $(u_m)_j^n$ and $(u_{mz})_j^n$, $m = 1$ and 2. These functions will be defined immediately.

According to Eq. (2a), $C = u_1 - \alpha u_2$ and it implies that

$$C_z = u_{1z} - \alpha u_{2z} \tag{12}$$

where the subscript 'z' means the partial derivative with respect to space ($\partial/\partial z$), as mentioned earlier. Combining

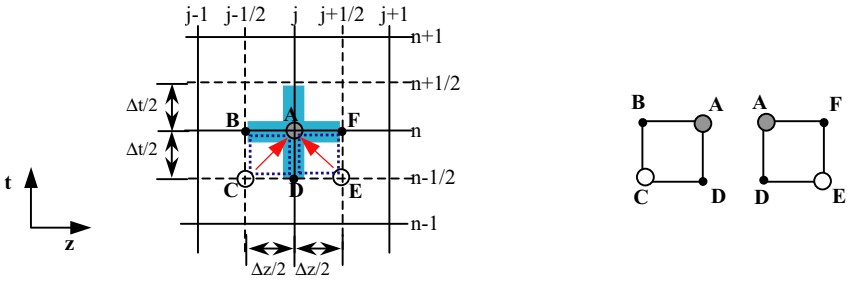

(a) Space-time staggered grid near SE(j,n) (b) CE$_-$(j,n) and CE$_+$(j,n)

Fig. 1. The solution element (SE) and conservation element (CE) at jth position and nth time level (Chang, 1995).

Eqs. (2b) and (12), one has:

$$f_1 = v_L(u_1 - \alpha u_2) - D_{ax}(u_{1z} - \alpha u_{2z}) \tag{13a}$$

$$f_{1z} = v_L(u_{1z} - \alpha u_{2z}) - \frac{\partial}{\partial z} D_{ax}(u_{1z} - \alpha u_{2z}) \tag{13b}$$

$$f_{1t} = v_L(u_{1t} - \alpha u_{2t}) - D_{ax}(u_{1t} - \alpha u_{2t}) \tag{13c}$$

An obvious numerical version of Eq. (13a) is:

$$(f_1)_j^n = v_L((u_1)_j^n - \alpha(u_2)_j^n) - D_{ax}((u_{1z})_j^n - \alpha(u_{2z})_j^n) \tag{14a}$$

Also, by neglecting the contribution from 2nd-order derivatives, the numerical versions of Eqs. (13b) and (13c) may be taken as:

$$(f_{1z})_j^n = v_L((u_{1z})_j^n - \alpha(u_{2z})_j^n) \tag{14b}$$

$$(f_{1t})_j^n = v_L((u_{1t})_j^n - \alpha(u_{2t})_j^n) \tag{14c}$$

In order that $(u_{mt})_j^n$, $m = 1$–3, can be determined in terms of $(u_{mz})_j^n$, $m = 1$–3, it is assumed that, for any $(z, t) \in \mathrm{SE}(j, n)$,

$$\nabla \cdot \tilde{h}_m(z, t; j, n) = 0, \quad m = 1\text{–}3 \tag{15}$$

Thus, within SE(j, n), the contribution of the source term (p_m) that appears in Eq. (3) is not modeled in Eq. (15). Note that (i) because it is the interior of a region that covers a horizontal line segment, a vertical segment and their immediate neighborhood, as mentioned earlier, SE(j, n) is a space–time region with infinitesimal small volume; and (ii) as will be shown, the contribution of source terms will be modeled in a numerical analogue of Eq. (5). With the aid of Eqs. (6)–(8), Eq. (15) implies:

$$(u_{mt})_j^n = -(f_{mz})_j^n, \quad m = 1\text{–}3 \tag{16}$$

Combining Eqs. (9)–(11), (14) and (16), one has:

$$(u_{1t})_j^n = -(f_{1z})_j^n = -v_L((u_{1z})_j^n - \alpha(u_{2z})_j^n) \tag{17}$$

$$(u_{2t})_j^n = -(f_{2z})_j^n = 0 \tag{18}$$

$$(u_{3t})_j^n = -(f_{3z})_j^n = 0 \tag{19}$$

Furthermore, with the aid of (17) and (18), Eq. (14c) and implies:

$$(f_{1t})_j^n = -v_L^2((u_{1z})_j^n - \alpha(u_{2z})_j^n) \tag{20}$$

Note that, by using Eqs. (10), (11), (14a), (14b), and (17)–(20), $(u_{mt})_j^n$, $(f_m)_j^n$, $(f_{mz})_j^n$ and $(f_{mt})_j^n$ can be determined explicitly in terms of $(u_m)_j^n$ and $(u_{mz})_j^n$.

2.2. Discretization of PDAEs

As in the construction of many other dissipative 1D CE/SE solvers, the current solver will be constructed without requiring that the conservation laws Eq. (5) be enforced numerically over both $\mathrm{CE}_-(j, n)$ and $\mathrm{CE}_+(j, n)$. Instead, Eq. (5) will be enforced only over CE(j, n).

To proceed, note that, in Fig. 1b, (i) $\overline{\mathrm{BF}}$ belongs to SE(j, n); (ii) $\overline{\mathrm{CB}}$ and $\overline{\mathrm{CD}}$ belong to $\mathrm{SE}(j - 1/2, n - 1/2)$; and (iii) $\overline{\mathrm{ED}}$ and $\overline{\mathrm{EF}}$ belong to $\mathrm{SE}(j + 1/2, n - 1/2)$. Thus, the boundary CE($j$, n) (i.e. the rectangle BCEF depicted in Fig. 1(a) and (b) is covered by the subsets of SE(j, n) and $\mathrm{SE}(j \pm 1/2, n - 1/2)$. As s result, it can be shown in Eq. (5) that approximated conservation fluxes, $\tilde{F}_j^n$, is:

$$(\tilde{F})_j^n \equiv \oint_{S(\mathrm{CE}(j,n))}^{\mathrm{c.c.}} (-\tilde{u}\,\mathrm{d}z + \tilde{f}\,\mathrm{d}t) \tag{21}$$

With the aid of Eqs. (6) and (7), the line integral in Eq. (21) results in for each component of $\tilde{F}_j^n$:

$$(\tilde{F}_m)_j^n = \tfrac{1}{2}\Delta z[2(u_m)_j^n - (u_m)_{j+1/2}^{n-1/2} - (u_m)_{j-1/2}^{n-1/2} + (s_m)_{j+1/2}^{n-1/2} - (s_m)_{j-1/2}^{n-1/2}], \quad m = 1\text{–}3 \tag{22}$$

where

$$(s_m)_{j\pm1/2}^{n-1/2} \overset{\mathrm{def}}{=} \frac{\Delta z}{4}(u_{mz})_{j\pm1/2}^{n-1/2} + \frac{\Delta t}{\Delta z}(f_m)_{j\pm1/2}^{n-1/2} + \frac{\Delta t^2}{4\Delta z}(f_{mt})_{j\pm1/2}^{n-1/2}, \quad m = 1\text{–}3 \tag{23}$$

In addition, approximated source term fluxes $(\tilde{P}_j^n)$ are obtained within V(CE(j, n)):

$$(\tilde{P})_j^n \equiv \int_V (p)_j^n\,\mathrm{d}V \tag{24}$$

The volume integral in Eq. (24) leads to for each component of $\tilde{P}_j^n$:

$$(\tilde{P}_m)_j^n = (p_m)_j^n \int_0^{\Delta z} \mathrm{d}z \int_0^{\Delta t/2} \mathrm{d}t = \frac{\Delta z\,\Delta t}{2}(p_m)_j^n, \quad m = 1\text{–}3 \tag{25}$$

In the current study, the numerical analogue of Eq. (5) will be taken as:

$$(\tilde{F}_m)_j^n = (\tilde{P}_m)_j^n, \quad m = 1\text{–}3 \tag{26}$$

With the aid of Eqs. (22) and (25), Eq. (26) implies that:

$$[2(u_m)_j^n - \Delta t(p_m)_j^n] - [(u_m)_{j+1/2}^{n-1/2} + (u_m)_{j-1/2}^{n-1/2} - (s_m)_{j+1/2}^{n-1/2} + (s_m)_{j-1/2}^{n-1/2}] = 0, \quad m = 1\text{–}3 \tag{27}$$

Using Eqs. (2) and (27), a discretized form of Eq. (1) is given within CE(j, n) as follows:

$$(u_1)_j^n = \tfrac{1}{2}[(u_1)_{j+1/2}^{n-1/2} + (u_1)_{j-1/2}^{n-1/2} - (s_1)_{j+1/2}^{n-1/2} + (s_1)_{j-1/2}^{n-1/2}] \tag{28a}$$

$$2(u_2)_j^n - \Delta tk((n^*)_j^n - (u_2)_j^n) = (u_2)_{j+1/2}^{n-1/2} + (u_2)_{j-1/2}^{n-1/2} - (s_2)_{j+1/2}^{n-1/2} + (s_2)_{j-1/2}^{n-1/2} \tag{28b}$$

$$g((u_1)_j^n - \alpha(u_2)_j^n, (n^*)_j^n) = 0 \tag{28c}$$

Obviously, by using Eq. (28a), $(u_1)_j^n$ can be determined explicitly in terms of the known mesh values at the (n –

1/2) time level. Eq. (28b) and the equation obtained by substituting the known value of $(u_1)_j^n$ into Eq. (28c) form a system of two nonlinear equations for $(u_2)_j^n$ and $(n^*)_j^n$. This system of equations can be solved by a Newton's iteration method.

Here, Δz and Δt are adjustable computation parameters. How their values should be chosen is problem-dependent. A small spatial step size (Δz) should be chosen for a problem associated with steep moving fronts. Also, a small CFL number ($\nu = v_L\,\Delta t/\Delta z$) is preferred for a problem that is stiff with respect to time.

As explained earlier, in addition to $(u_m)_j^n$, $m = 1$–3, at each mesh point (j, n), the independent discrete variables to be solved also include $(u_{mz})_j^n$, $m = 1$–3. Because $(u_3)_j^n \equiv 0$ and $(u_{3z})_j^n \equiv 0$, in the following, we will describe how $(u_{mz})_j^n$, $m = 1$ and 2, can be evaluated in terms of known values of $(u_m)_{j\pm1/2}^{n-1/2}$, $(u_{mz})_{j\pm1/2}^{n-1/2}$ and $(u_m)_j^n$, $m = 1$ and 2.

To proceed, note that the stability of a CE/SE scheme requires that the CFL number $\nu < 1$ (Chang, 1995). Without using special techniques that involve ad hoc parameters, generally the numerical dissipation associated with a CE/SE simulation with a fixed total marching time increases as the CFL number decreases. As a result, for a small CFL number (say $\nu < 0.1$), a CE/SE scheme may become overly dissipative. To overcome this shortcoming, a new CFL number insensitive scheme, i.e. the so called Scheme II, was introduced in Chang (2002). The new scheme differs from other CE/SE schemes only in how $(u_{mz})_j^n$ is evaluated. According to Scheme II, we have:

$$(u_{mz})_j^n = \frac{[1 + f(|\nu|)(r_{m-})_j^n](\hat{u}_{mz+})_j^n + [1 + f(|\nu|)(r_{m+})_j^n](\hat{u}_{mz-})_j^n}{2 + f(|\nu|)[(r_{m-})_j^n + (r_{m+})_j^n]}, \quad m = 1, 2 \tag{29}$$

where

$$f(|\nu|) \stackrel{\text{def}}{=} \frac{0.5}{|\nu|} \tag{30}$$

$$(r_{m\pm})_j^n \stackrel{\text{def}}{=} \frac{|(\hat{u}_{mz\pm})_j^n|}{\min(|(\hat{u}_{mz+})_j^n|, |(\hat{u}_{mz-})_j^n|)} - 1, \quad m = 1, 2 \tag{31}$$

$$(\hat{u}_{mz\pm})_j^n = \frac{4}{\Delta z}\frac{\mp(u_m)_j^n \pm [(u_m)_{j\pm1/2}^{n-1/2} + (\Delta t/2)(u_{mt})_{j\pm1/2}^{n-1/2}] \mp((1 - |\nu|)\Delta z/4)(u_{mz})_{j\pm1/2}^{n-1/2}]}{1 + |\nu|}, \quad m = 1, 2 \tag{32}$$

Here, as explained in Chang (2002), for each m, (i) $(\hat{u}_{mz+})_j^n$ and $(\hat{u}_{mz-})_j^n$ can be considered as the spatial derivatives of u_m at the point (j, n) evaluated from the right and the left, respectively; and (ii) the expression on the right side of Eq. (29) represents an weighted average of $(\hat{u}_{mz+})_j^n$ and $(\hat{u}_{mz-})_j^n$.

Eq. (32) is reduced for Eq. (1b) with the aid of Eq. (18) into:

$$(\hat{u}_{2z\pm})_j^n = \frac{4}{\Delta z}\frac{\mp(u_2)_j^n \pm [(u_2)_{j\pm1/2}^{n-1/2} \mp((1 - |\nu|)\Delta z/4)(u_{2z})_{j\pm1/2}^{n-1/2}]}{1 + |\nu|} \tag{33}$$

Note that, because $(u_3)_j^n = (u_{3z})_j^n = 0$, the only independent discrete variables at any mesh point (j, n) are $(u_m)_j^n$ and $(u_{mz})_j^n$, $m = 1$ and 2, which can be evaluated using Eqs. (28) and (29).

Consequently, the present CE/SE method with Eqs. (27) and (28) leads to a PDAE system which, at each time level, is associated with a block diagonal Jacobian matrix. Let the number of mesh points be N_{mesh}. The maximum number of non-zero Jacobian elements for the CE/SE method, $J_{\max}^{\text{CE/SE}}$, is in Eq. (1):

$$J_{\max}^{\text{CE/SE}} = (3 \times 3) \times N_{\text{mesh}} \tag{34a}$$

In the case of linear source terms or without the source term, the Jacobian matrix is further reduced to a diagonal form:

$$J_{\min}^{\text{CE/SE}} = (1 \times 1) \times N_{\text{mesh}} \tag{34b}$$

For Eq. (1), a band matrix is obtained, when a DAE integrator is used in the framework of the method of lines (MOL). Let the length of the upper and lower band matrix be MU and ML, which depend on the size of spatial discretization and nonlinearity of the PDAE considered. The maximum number of non-zero band-Jacobian elements for the MOL is known as for $m = 3$:

$$J_{\max}^{\text{MOL}} = 3N_{\text{mesh}}(\text{ML} + \text{MU} + 1) - \tfrac{1}{2}\text{ML}(\text{ML} + 1) - \tfrac{1}{2}\text{MU}(\text{MU} + 1) \tag{35a}$$

For example, in the simplest case that the convection term is discretized by a 1st-order backward scheme and the diffusion term by a central scheme in Eq. (1), ML = MU = 3. The smallest number of non-zero Jacobian elements in this case, $J_{\min}^{\text{MOL}}$, can be approximated for the state variable (u) and its time derivative ($\mathrm{d}u/\mathrm{d}t$) at each time step:

$$J_{\min}^{\text{MOL}} \approx (3 \times 3) \times N_{\text{mesh}} \tag{35b}$$

As a result, the following relation can be derived:

$$J_{\min}^{\text{CE/SE}} < J_{\max}^{\text{CE/SE}} = J_{\min}^{\text{MOL}} \le J^{\text{MOL}} \tag{36}$$

Eq. (36) means that the number of non-zero Jacobian elements for the MOL, J^{MOL}, is not less than $J_{\max}^{\text{CE/SE}}$. The computational time is normally proportional to the number of non-zero Jacobian elements (J) multiplied by the number of time steps (N_{time}), i.e. $J \times N_{\text{time}}$. Therefore, it is expected that the computational time of the CE/SE method is shorter than the MOL under the condition of the same number of time steps. Especially for non-stiff systems (e.g. chromatographic adsorption problems), the CE/SE method will save

the computational time because the small number of time steps can be used.

The stability of the CE/SE method is limited only by the Courant–Friedrichs–Lewy (CFL) condition (Chang, 1995), as mentioned earlier. If the fluid velocity (v_L) is given, the condition is expressed in term of the CFL number ($\nu = v_L\,\Delta t/\Delta z$):

$$0 < |\nu| < 1 \tag{37}$$

While the implicit DAE integrator has self-adaptive feature about the time step size (Δt), the present CE/SE method has a fixed value of Δt satisfying the CFL condition.

2.3. Boundary condition treatment

Boundary conditions (at $j = 1$ and N_{mesh}) for state variables (u) and its spatial derivatives (u_z) are needed only at each integer-time level ($n = 0, 1, 2, 3, \ldots$) in the space–time CE/SE method. At each half-time level ($n = 1/2,\ 1 + 1/2,\ 2 + 1/2,\ \ldots$), these values ($u$ and u_z) for all mesh points ($j = 1 + 1/2, 2 + 1/2, \ldots, N_{mesh} - 1/2$) are calculated on the basis of these values of the previous time level (i.e. integer-time level) without boundary values. Note that the CE/SE method has a staggering mesh structure and intrinsically space–time triangle computational elements.

Without particular boundary conditions, the two boundary conditions of first and last spatial points ($z = 0$ and $z = L_c$) at each integer-time level are assumed as follows (for simplicity, subscript 'm' of u_m and u_{mz} is omitted):

$$\text{At } z = 0, \quad u_1^n = u_{1+1/2}^{n-1/2}, \qquad (u_z)_1^n = (u_z)_{1+1/2}^{n-1/2} \tag{38a}$$

$$\text{At } z = L_c, \quad u_{N_{mesh}}^n = u_{N_{mesh}-1/2}^{n-1/2}, \quad (u_z)_{N_{mesh}}^n = (u_z)_{N_{mesh}-1/2}^{n-1/2} \tag{38b}$$

The above equations mean that the first and last boundary values ($u_1^n, u_{N_{mesh}}^n, (u_z)_1^n$ and $(u_z)_{N_{mesh}}^n$) at the present time level (t^n) are estimated by the first and last values ($u_{1+1/2}^{n-1/2}, u_{N_{mesh}-1/2}^{n-1/2}, (u_z)_{1+1/2}^{n-1/2}$ and $(u_z)_{N_{mesh}-1/2}^{n-1/2}$) at the previous time level ($t^{n-1/2}$).

Suppose that a boundary condition for Eq. (1a) is imposed as below:

$$\text{At } z = 0 \text{ and } \forall t, \quad v_L(C_1 - C_{in}) = D_{ax}(C_z)_1 \tag{39a}$$

$$\text{At } z = L_c \text{ and } \forall t, \quad (C_z)_{N_{mesh}} = 0 \tag{39b}$$

where C_{in} is a known feed concentration just before entering to the column. Due to Eq. (39a) or Eq. (39b), one value of the two boundary values (u_1^n and $(u_z)_1^n$ or $u_{N_{mesh}}^n$ and $(u_z)_{N_{mesh}}^n$) remains unknown and must be assumed or given by the user. A simple assumption is applied for Eq. (39) as follows:

$$\text{At } z = 0 \text{ and } n = 1, 2, 3, \ldots, \quad v_L(C_1^n - C_{in}) = D_{ax}(C_z)_1^n, \qquad (C_z)_1^n = \frac{C_2^n - C_{in}}{2\Delta z} \tag{40a}$$

$$\text{At } z = L_c \text{ and } n = 1, 2, 3, \ldots, \quad C_{N_{mesh}}^n = C_{N_{mesh}-1}^n, \qquad (C_z)_{N_{mesh}}^n = 0 \tag{40b}$$

Note that $C_1^n = (u_1)_1^n - \alpha(u_2)_1^n$ in Eq. (40a) is calculated linearly since $C_2^n = (u_1)_2^n - \alpha(u_2)_2^n$ can independently be obtained from Eq. (28).

For a recycle flow, consider a boundary condition instead of Eq. (39a):

$$\text{At } z = 0 \text{ and } \forall t, \quad v_L(C_1 - C_{out}) = D_{ax}(C_z)_1 \tag{41}$$

where C_{out} is the outlet fluid concentration at $z = L_c (j = N_{mesh})$. The condition is represented on discrete points instead of Eq. (40a):

$$\text{At } z = 0 \text{ and } n = 1, 2, 3, \ldots, \quad v_L(C_1^n - C_{N_{mesh}}^n) = D_{ax}(C_z)_1^n, \quad (C_z)_1^n = \frac{C_2^n - C_{N_{mesh}}^n}{2\Delta z} \tag{42}$$

Since $C_{N_{mesh}}^n = (u_1)_{N_{mesh}}^n - \alpha(u_2)_{N_{mesh}}^n$ is also obtained independently from Eq. (40b), C_1^n can be calculated directly. Therefore, the boundary condition treatment (or recycle flow handling) does not break the form of the block diagonal Jacobian matrix, which is of great advantage to the MOL that often leads to a sparse Jacobian matrix for the handling of recycle flows.

3. Numerical studies

Two examples are tested. The first example is an one-component chromatographic model with a linear adsorption isotherm to reveal the properties of the CE/SE method in comparison to the standard MOL (method of lines). The system can simply be reduced to a PDE system including one PDE and one ODE. However, a model in the PDAE form is numerically solved with or without axial dispersion on 21 or 201 mesh points. The second example is a two-component chromatographic model with non-linear adsorption isotherms, which is also a PDAE system.

In the CE/SE method, the Newton–Rhapson algorithm is employed to solve a system of nonlinear equations. The absolute and relative tolerances for convergence are both equal to 1.0×10^{-5} and 3–4 iterations are needed for a satisfactory convergence.

For comparison with the CE/SE method, a Backward Differentiation Formulae (BDF) DAE time integrator (Petzold, 1983) in the framework of the MOL (hereafter it is called the MOL) is used with several spatial discretization methods. The convection term (1st-order spatial derivative) is discretized by a two-point backward upwinding scheme (1st-order upwind), a two-point central scheme (2nd-order central), a six-point upwinding scheme (5th-order upwind), a 3rd-order WENO upwinding scheme on a flexible stencil (3rd-order WENO) and a 5th-order WENO upwinding scheme on a flexible stencil (5th-order WENO). For the

diffusion term (2nd-order spatial derivative), a two-point central discretization is employed. The detailed formulas are presented in Lim et al. (2001a). All the resulting DAE systems are characterized by a band Jacobian matrix which is numerically evaluated. In the BDF DAE integrator, the absolute and relative tolerances are set equally to 1.0×10^{-5} for first example and 1.0×10^{-4} for the second example.

All simulations are performed on a single 1.3 GHz Athlon processor equipped with 516 RAM. The computational time (or CPU time) is the time required for a single task in the computer. Accuracy is measured at a moment (t) or at a position (z) by the L_1-error defined as follows:

$$L_1\text{-error} = \sum_{i=1}^{N_{\text{mesh}}(\text{or } N_{\text{time}})} \times |(u_i)_{\text{reference}} - (u_i)_{\text{computed}}| \, \Delta z(\text{or } \Delta t) \quad (43)$$

where $(u_i)_{\text{reference}}$ is the high-accuracy numerical (reference) solution and $(u_i)_{\text{computed}}$ is numerical solutions evaluated by the MOL or the CE/SE method. Instability is indicated by spurious oscillatory behavior in the numerical solutions.

3.1. One-component chromatographic model with a linear adsorption isotherm

The packed-bed chromatographic problem, Eq. (1), is solved for one component with the volume ratio $\alpha = 1.5$, the fluid velocity $v_L = 0.1$ m/s, the axial dispersion coefficient $D_{ax} = 0$ or 1.0×10^{-5} m^2/s, and the adsorption rate coefficient $k = 0.0129\,\text{s}^{-1}$. A linear adsorption isotherm is used for the algebraic equation of Eq. (1c).

$$n^* = 0.85C \quad (44)$$

The column length is the interval $0 \le z \le 1.5$ and the integration time is $0 \le t \le 10$ s. As the initial condition, $C(0, z) = 0$, $n(0, z) = 0$ and $n^*(0, z) = 0$ for all z except $z = 0$ and $z = L_c$. The two boundary conditions ($z = 0$ and $z = L_c$) are given in Eq. (39).

First, Eq. (1) without the diffusion term is solved ($D_{ax} = 0$) and with a step input concentration at $z = 0$ ($C_{in} = 2.2$ for $t \ge 0.0$). In the second and third tests, the diffusion term is included with $D_{ax} = 1.0 \times 10^{-5}$. Here an inlet square concentration pulse is considered as follows:

$$C_{in} = 2.2, \quad \text{for} \quad 0\,\text{s} \le t \le 2.0\,\text{s} \quad (45a)$$

$$C_{in} = 0.0, \quad \text{for} \quad 2.0\,\text{s} \le t \le 10.0\,\text{s} \quad (45b)$$

The numerical solutions are obtained on 201 or 21 equidistant spatial mesh points. The CFL number for the CE/SE method is given at $\nu = 0.4$.

In the first case (no diffusion and 201 mesh points), the high-accuracy reference solution is obtained using a 5th-order WENO scheme on 301 mesh points (see Lim et al., 2001a). In the second or third case (diffusion and 201 or 21 mesh points), the reference solution is obtained on 401 mesh points through the CE/SE method, where the calculation time was 4.1 s.

Table 1
Accuracy, temporal performance and stability evaluation for a chromatographic adsorption PDAE without axial dispersion on 201 mesh points

		Accuracy (L_1 error)[a]	CPU time (s)[b]
MOL	1st-order upwind	0.1307	0.9
	2nd-order central	0.1140[c]	1.3
	5th-order upwind	0.0218[c]	2.3
	3rd-order WENO	0.0426	5.9
	5th-order WENO	0.0252	9.5
CE/SE Scheme II (CFL = 0.4)	Newton iteration	0.0185	1.2

[a] L_1 error at $t = 10$ s.
[b] CPU time during 10 s integration time.
[c] Unstable numerical solution.

Table 2
Accuracy, temporal performance and stability evaluation for a chromatographic adsorption PDAE with axial dispersion and square input concentration on 201 mesh points

		Accuracy (L_1 error)[a]	CPU time (s)[b]
MOL	1st-order upwind	0.2075	1.6
	2nd-order central	0.0979[c]	1.9
	5th-order upwind	0.0060[c]	2.9
	3rd-order WENO	0.0449	7.7
	5th-order WENO	0.0168	11.3
CE/SE Scheme II (CFL = 0.4)	Newton iteration	0.0087	1.3

[a] L_1 error at $t = 10$ s.
[b] CPU time during 10 s integration time.
[c] Unstable numerical solution.

Tables 1–3 report numerical performance on accuracy, computational efficiency and stability for the chromatographic adsorption problem without or with axial dispersion on 201 or 21 mesh points. The 2nd-order central and 5th-order upwinding schemes give spurious oscillatory solutions near steep regions. Thus, the two methods seem to be inadequate for convection-dominated problems as

Table 3
Accuracy, temporal performance and stability evaluation for a chromatographic adsorption PDAE with axial dispersion and square input concentration on 21 mesh points

		Accuracy (L_1 error)[a]	CPU time (s)[b]
MOL	1st-order upwind	0.5423	0.04
	2nd-order central	0.5430[c]	0.04
	5th-order upwind	0.2385[c]	0.06
	3rd-order WENO	0.4250	0.14
	5th-order WENO	0.2945	0.12
CE/SE Scheme II (CFL = 0.4)	Newton iteration	0.2450	0.02

[a] L_1 error at $t = 10$ s.
[b] CPU time during 10 s integration time.
[c] Unstable numerical solution.

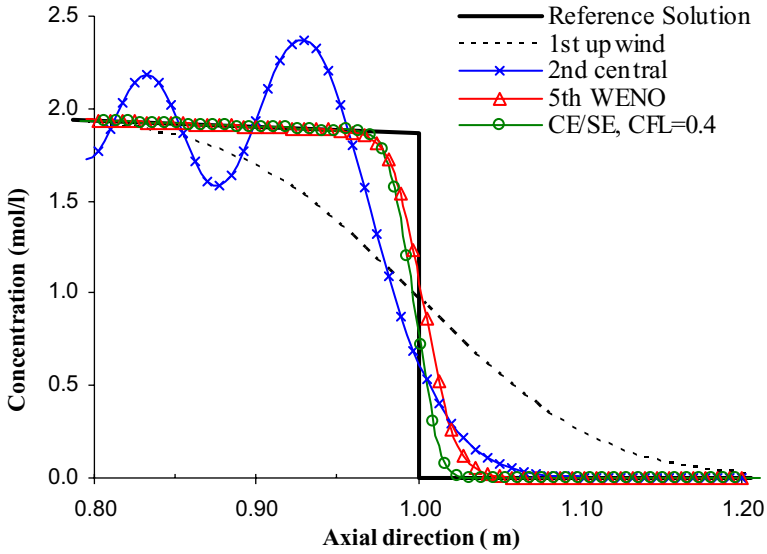

Fig. 2. Fluid concentration (C) profiles according to numerical schemes near $z = 1.0$ at $t = 10$ s for a chromatographic adsorption problem without axial dispersion ($D_{ax} = 0$) on 201 mesh points.

mentioned in Lim et al. (2001a). The 1st-order upwinding scheme (called 1st-order upwind) is not accurate because of its low order of accuracy. The two WENO schemes (3rd-order and 5th-order) enhance accuracy and stability but at the cost of longer computation time. The CE/SE method gives, in the three case studies, the most accurate solution with very short calculation times in a stable manner.

In Fig. 2, numerical solutions of the fluid concentration (C) are depicted near $z = 1.0$ at $t = 10$ s for the adsorption problem without axial dispersion. Its reference solution is a discontinuous profile at $z = 1$. The CE/SE method shows the best solution without spurious oscillation of the six schemes tested. A smeared peak is shown for the problem with dispersion in Fig. 3. As expected, 1st-order upwind is not accurate and 2nd-order central is highly oscillatory. The MOL with 5th-order WENO and the CE/SE with CFL = 0.4 exhibit similar resolution in steep regions without spurious oscillations.

On the 21 mesh points, numerical solutions are much less accurate than those on the 201 mesh points (see Fig. 4). However, it takes much less computational time, as reported in Table 3. The 5th-order upwinding scheme seems to be most accurate but gives spurious solutions, showing negative concentrations before and after steep fronts.

One of the advantages for the CE/SE method is that the numerical error does not accumulate with respect to time and space at a fixed CFL number (or a space–time flux conservation feature), as mentioned above. Whereas, the error

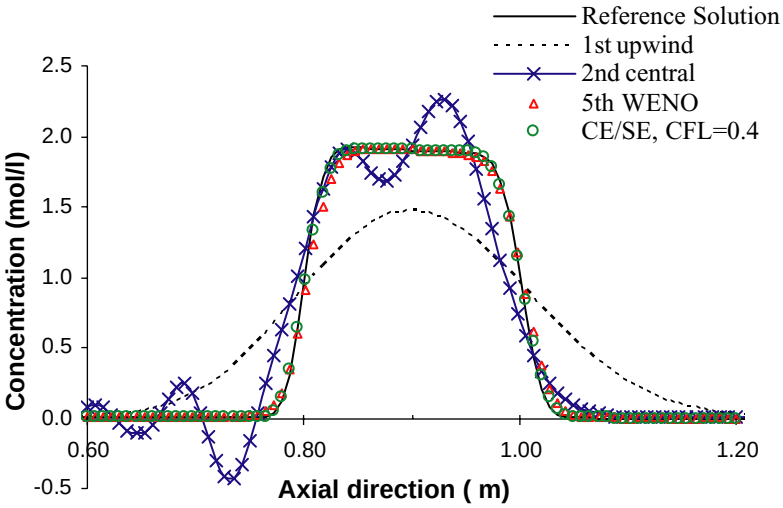

Fig. 3. Fluid concentration (C) profiles for different numerical schemes around $z = 0.9$ at $t = 10$ s for the single component chromatographic adsorption problem with axial dispersion ($D_{ax} = 1.0 \times 10^{-5}$) and square input concentration on 201 mesh points.

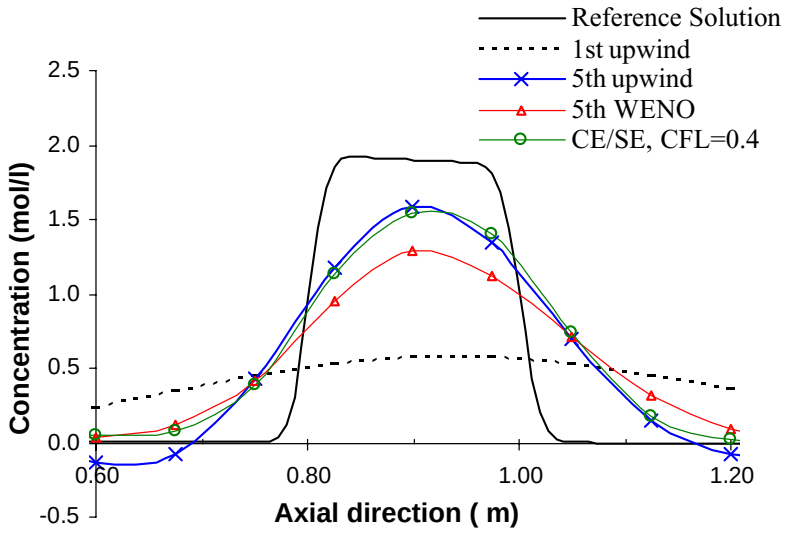

Fig. 4. Fluid concentration (C) profiles for different numerical schemes around $z = 0.9$ at $t = 10$ s for the single component chromatographic adsorption problem with axial dispersion ($D_{ax} = 1.0 \times 10^{-5}$) and square input concentration on 21 mesh points.

is amplified with time in traditional discretization schemes (e.g. 1st-order upwind, 2nd-order central, and 5th-order upwind) in the framework of the MOL. Since the WENO schemes for 1D problems are constructed by a finite volume approach, these schemes are also non-dissipative with time. Fig. 5 shows the propagation of steep waves with time for the second case on 201 mesh points. Note that the 5th-order WENO scheme (circles) and the CE/SE method (solid line)

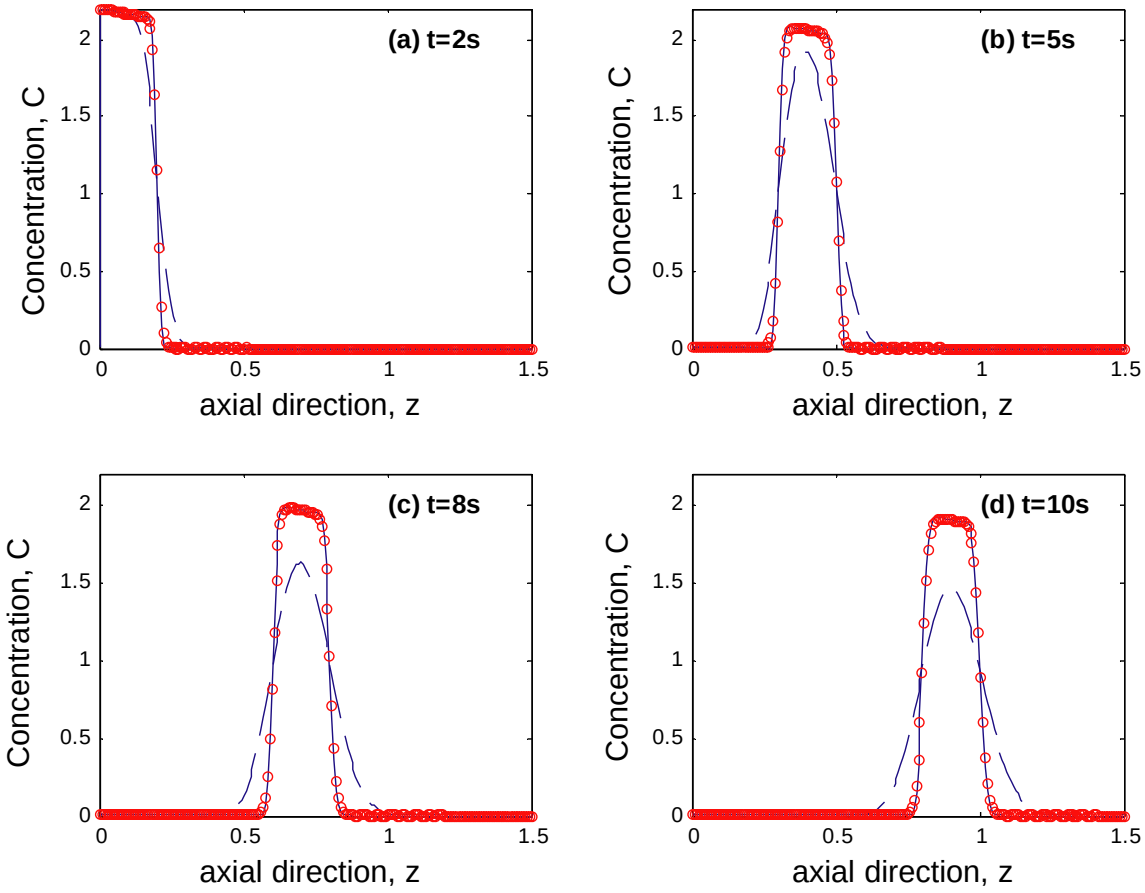

Fig. 5. Fluid concentration (C) propagation with time for a chromatographic adsorption problem with axial dispersion on 201 mesh points (dashed line: 1st-order upwind, circles: 5th-order WENO, solid lines: CE/SE with CFL = 0.4).

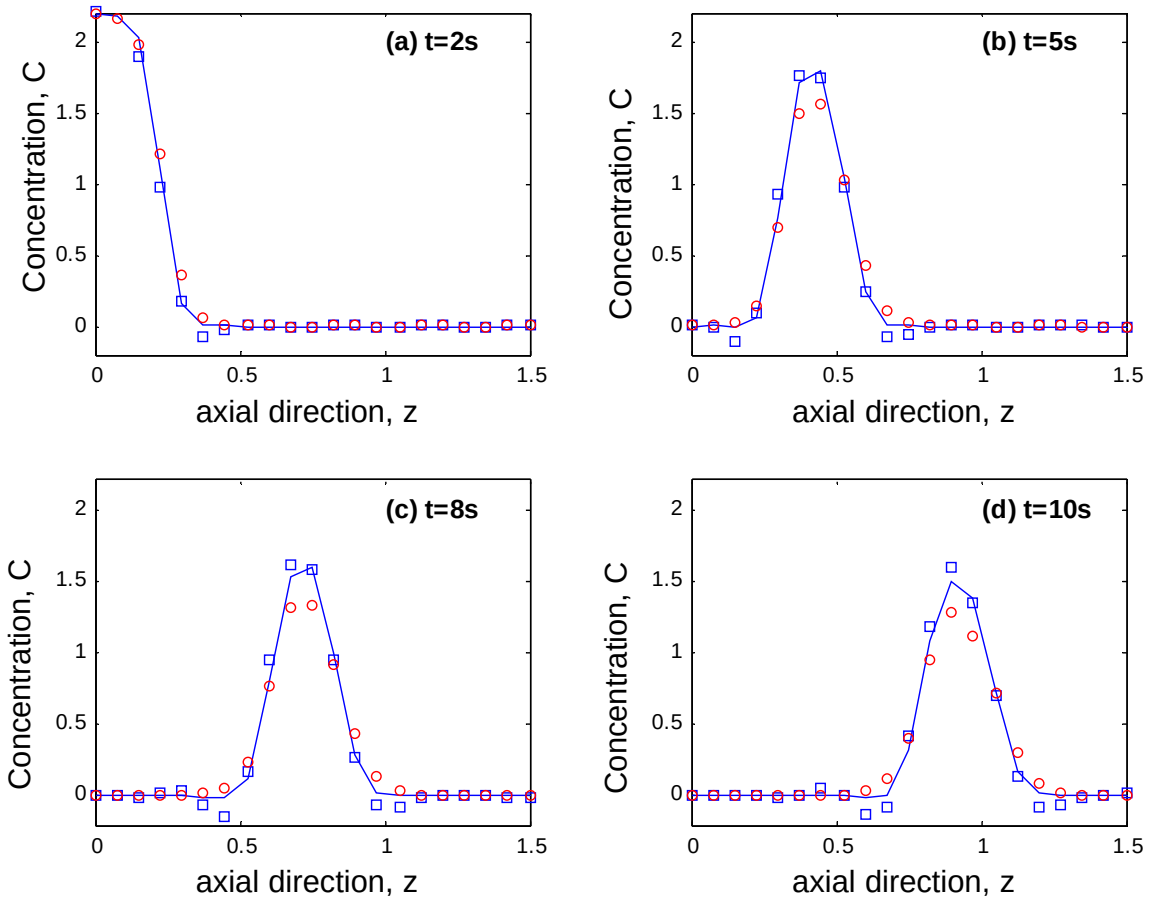

Fig. 6. Fluid concentration (C) propagation with time for a chromatographic adsorption problem with axial dispersion on 21 mesh points (dashed line: 1st-order upwind, circles: 5th-order WENO, solid lines: CE/SE with CFL = 0.4).

have a non-dissipative feature, since the waves do not widen with time. In contrast, the peak of the 1st-order upwinding scheme (dashed line) broadens continually as time increases.

Fig. 6 depicts the wave propagation on 21 mesh points. The oscillatory behavior of the 5th-order upwind scheme (squares) is clear. The CE/SE method (solid line) is superior in accuracy to the 5th-order WENO scheme (circles) for all times.

3.2. Two-component chromatographic model with nonlinear adsorption isotherms

An anion-exchange preparative chromatography is considered in an isocratic mode for Bovine Serum Albumin (BSA) protein separation. A non-linear equilibrium (or isotherm) model (Li & Pinto, 1995; Raje & Pinto, 1997) is used to describe non-ideal solution behaviors for salts in the liquid phase using an extended Debye–Hückel model (Bromley, 1973) and non-ideality for proteins and salts in the solid phase using a spreading-pressure-dependent equation (Talu & Zwiebel, 1986).

In Appendix A, the adsorption isotherm model is presented and the model parameters are given for the BSA–NaCl system. The experimental data for the adsorption isotherms (Li & Pinto, 1995) are compared in Fig. 7 with results predicted by the model. The adsorption isotherms are predicted for $C_{\mathrm{NaCl}} = 0.207$ mol/l within a reasonable error bound.

Table 4 shows design, operation and simulation parameters used in this numerical study. Since solid concentrations (n_i and n_i^*) have the units (mmol/kg-resin), the phase ratio (α) in Eq. (1a) is defined as:

$$\alpha = \frac{1-\varepsilon_{\mathrm{b}}}{\varepsilon_{\mathrm{b}}}\rho_{\mathrm{r}} \tag{46}$$

where ε_{b} is the bed voidage and ρ_{r} the resin density with the value given in Table 4. The resin is initially saturated with chloride ions (Cl^-). Note that mass transfer coefficient (k) should have the same value for the two components (BSA and Cl^-) in order to satisfy the electro-neutrality condition.

$$n_{\mathrm{T}} = n_1(z_1 + \sigma z_2) + z_2 n_2 \tag{47}$$

where n_{T} is the total resin capacity, z_1 and z_2 are the ion valences for BSA and Cl^-, respectively. σ is the steric factor for the BSA–NaCl system. Note that Eq. (47) in the solid phase corresponds to Eq. (A.6) on the interface or resin surface (see Appendix A).

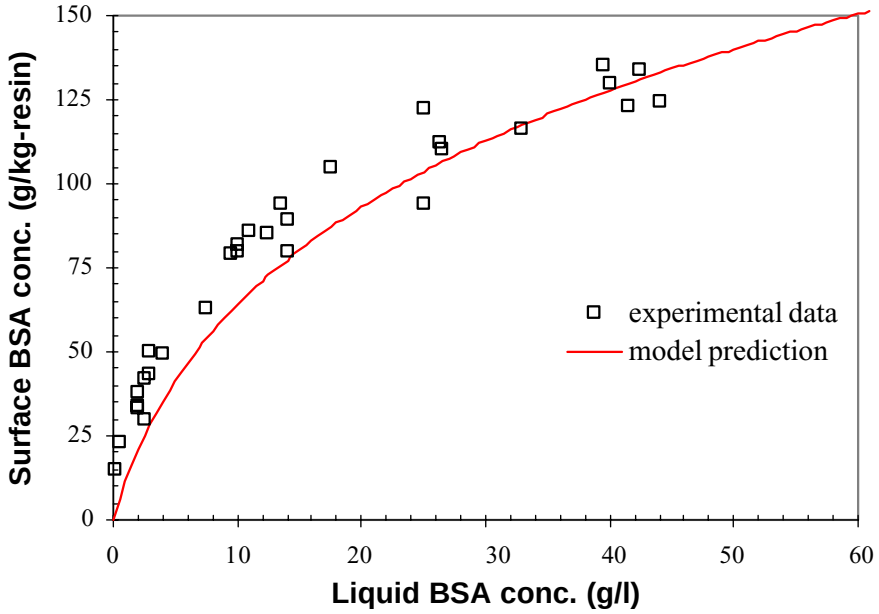

Fig. 7. Experimental data in Li and Pinto (1995) and model prediction ($m = 18.0$ and $\sigma = 24.0$) for BSA equilibrium isotherms at $C_{NaCl} = 0.207$ mol/l.

Replacing Eq. (1c) with Eq. (A.13) involving Eqs. (A.1)–(A.12), the resulting PDAE system to be solved contains two PDEs, two ODEs and two AEs. That is, Eq. (2) is reformulated:

$$u = \begin{pmatrix} C_1 + \alpha n_1 \\ n_1 \\ 0 \\ C_2 + \alpha n_2 \\ n_2 \\ 0 \end{pmatrix} \tag{48a}$$

$$f = \begin{pmatrix} v_L C_1 - D_{ax}\dfrac{\partial C_1}{\partial z} \\ 0 \\ 0 \\ v_L C_2 - D_{ax}\dfrac{\partial C_2}{\partial z} \\ 0 \\ 0 \end{pmatrix} \tag{48b}$$

$$p = \begin{pmatrix} 0 \\ k(n_1^* - n_1) \\ g_1(C_1, C_2, n_1^*, n_2^*) \\ 0 \\ k(n_2^* - n_2) \\ g_2(C_1, C_2, n_1^*, n_2^*) \end{pmatrix} \tag{48c}$$

where subscripts '1' and '2' means component-1 (BSA) and component-2 (Cl^-), respectively. Thus, $C_1 = u_1 - \alpha u_2$ and $C_2 = u_4 - \alpha u_5$. The model parameters are given in Table 4.

The system of equations discretized in the framework of the CE/SE method leads to a (6×6) block diagonal Jacobian matrix of the length N_{mesh} at each time level ($J_{max}^{CE/SE} = (6 \times 6) \times N_{mesh}$). Each block Jacobian matrix which contains non-linear coupling terms between its elements is evaluated for solving the equation system through the Newton–Rhapson algorithm, numerically evaluating derivatives of the source term (dp/du).

Table 4
Design, operation and simulation parameters in a BSA ion-exchange preparative chormatography

Design parameters		Operating conditions		Simulation parameters	
L_c (cm)	25	Q (ml/min)	1	k (min^{-1})	$k_1 = k_2 = 6.0$
i.d. (cm)	0.46	v_L (cm/min)	7.57	D_{ax} (cm^2/min)	1.89×10^{-4}
ε_b	0.7947	T (°C)	35.4	N_{mesh}	201
n_T (meq./kg-resin)	360	C_0 (mmol/l) n_0 (meq./kg-resin)	$C_1 = 0$, $n_1 = 0$ $C_2 = 207$, $n_2 = n_T$[a]	ν ($=v_L(\Delta t/\Delta z)$)	0.73
ρ_r (kg/l-resin)	3.65[b]	C_{in} (mmol/l)	$C_1 = 0.889$, $C_2 = 207$ for $0\,s \le t \le 0.5\,s$ $C_1 = 0$, $C_2 = 207$ for $0.5\,s \le t \le 60\,s$	t (min)	60

[a] 1st-component: BSA, 2nd-component: NaCl.
[b] Wet resin density (ρ_r) is based on the particle volume including the pore volume.

Table 5
Accuracy, temporal performance and stability evaluation for a BSA ion-exchange chromatography on 201 mesh points

		Accuracy (L_1 error)[a]	CPU time (min)[b]
MOL	1st-order upwind	2.629	95
	2nd-order central	–[c]	–
	5th-order upwind	1.063[d]	140
	3rd-order WENO	1.361	460
	5th-order WENO	0.551	710
CE/SE Scheme II (CFL = 0.73)	Newton iteration	0.638	15

[a] L_1 error at $z = 25$ cm.
[b] Rounding-off CPU time during 60 min integration time.
[c] No convergence.
[d] Unstable numerical solution.

In the framework of the MOL, the band Jacobian matrix is constructed with $ML = (6-1) \times N_{mesh}$ and $MU = (6-3) \times N_{mesh}$ for all discretization methods. Using Eq. (35a), the maximum number of non-zero Jacobian elements is $J_{max}^{MOL} = (31N_{mesh} + 2)N_{mesh}$. However, it would be adequate for the Jacobian matrix to be constructed by the sparse matrix technique rather than the band matrix, because the actual number of non-zero elements inside the band matrix (J^{MOL}) is less than 1% of J_{max}^{MOL}. In this study, since the band Jacobian is numerically evaluated because of the complex adsorption isotherm model, much longer computational time will be required for the MOL. The number of mesh points is $N_{mesh} = 201$ equally for the CE/SE method and the MOL.

In the two-component ion-exchange problem, Table 5 shows the CPU time for simulation of 60-min operation time and accuracy of solutions at $z = 25$ cm for 60 min. To evaluate the accuracy, the reference solution is obtained from the CE/SE method on 401 mesh points with $\nu = 0.727$, where the computational time is about 60 min. Even though the Jacobian of the adsorption isotherm is numerically evaluated for the CE/SE method, its computational time is much faster than those of the five different MOL due to the small size of the block diagonal Jacobian matrix.

The 2nd-order central discretization scheme (2nd-order central) does not give reliable solutions, because substantial oscillations of liquid concentrations including negative values lead to non-convergence in solving Eq. (A.13). The 5th-order upwinding scheme (5th-order upwind) also produces some oscillatory behavior (see Fig. 8) and its accuracy is not substantially improved. The two WENO schemes guarantee non-oscillatory solutions but require long computational times. It is interesting that solution accuracy of the 5th-order WENO scheme is comparable to that of the CE/SE method. However, solutions of the CE/SE method are obtained with much faster computational time.

The peak shape of the breakthrough curve is characterized by a sharpening front and tailing rear. In Fig. 8, the breakthrough curves at $z = 25$ cm (or the exit of the column) are depicted according to the numerical schemes. As stated earlier, an overshoot is appearing near maximum concentrations in the 5th-order upwinding scheme. The 5th-order WENO scheme and the CE/SE method with $\nu = 0.727$ show good agreement with the reference solution. It is worth noting that the chromatographic adsorption problem is not stiff but demonstrates steep fronts, and a high CFL number (ν) can be used.

In Fig. 9, the salt and total liquid concentrations are shown on the basis of the equivalent molar concentration (meq./l). If the hindered salt ion ratio in the steric mass-action model (Brooks & Cramer, 1992) is equal to zero ($\sigma = 0$), the salt concentration would be constant at $C_{NaCl} = 207$ meq./l and the total concentration ($C_{BSA} + C_{NaCl}$) would mimic the profile of the BSA liquid concentration in Fig. 8. However, since salt ions (Cl^-) are sterically hindered on the surface of resin particles by adsorbed BSA proteins, the salt liquid concentration decreases and the chloride ions are bound within the resin.

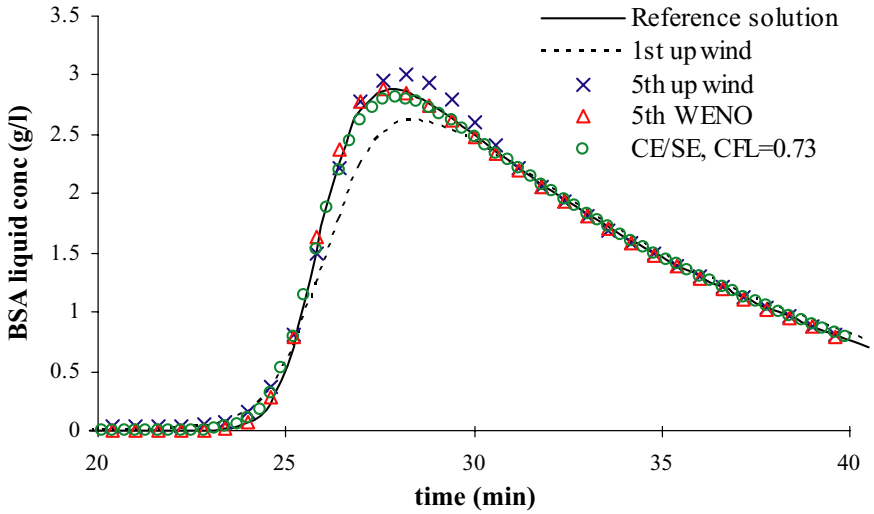

Fig. 8. Breakthrough curve of the protein (BSA) according to numerical schemes for the BSA–NaCl ion-exchange problem.

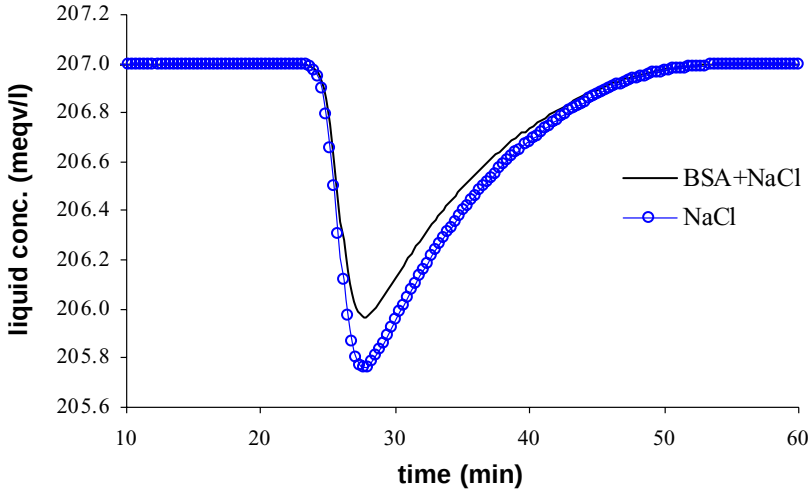

Fig. 9. Breakthrough curve of the total liquid concentration (BSA + NaCl) and the salt (NaCl) for the BSA–NaCl ion-exchange problem.

4. Conclusion

In this paper, the space–time CE/SE method is extended to solve partial differential algebraic equation (PDAE) systems, by including a Newton iterative method for solving nonlinear algebraic equations. The CE/SE method is compared with the MOL with high accuracy upwinding schemes in terms of accuracy, computational performance and occurrence of spurious solutions for chromatographic separation problems described by a non-stiff PDAE system.

In the case studies presented, the current CE/SE scheme has the best numerical performance among the six test schemes. This feat, at least partially, is due to the fact that the CE/SE method enforces flux conservation in space–time and, therefore, is inherently adept at resolving steep or shock moving fronts. The current CE/SE scheme is also easy to implement because, using a space–time mesh, the convection, diffusion and reaction terms can be discretized in a straightforward manner. For stability, the spatial mesh interval and the time step size specified may need to satisfy the CFL condition only. However, to meet accuracy requirement, they may be subjected to stricter constraints. This is particularly true when the system is stiff. As such, an effort to extend the current scheme for application to stiff chromatographic adsorption problems is under way.

Finally noted that, because the current study represents the first application of the CE/SE method to chromatographic adsorption problems, the CE/SE algorithm presented here must be considered as a scheme still in its earlier stage of development. Thus, in spite of the promising numerical results presented, the advantages and disadvantages of the CE/SE method (as compared with other established methods) can only be evaluated objectively through future studies.

Appendix A

The bovine serum albumin (BSA) showing pI = 4.7–4.9 and $M_w \approx 69$ kDa (Raje & Pinto, 1997) is adsorbed on a weak anion resin (Matrex PAE-1000) in an isocratic mode ($C_{NaCl} = 207$ mmol/l). For the anion-exchange between BSA and Cl^-, the mass action law (or equilibrium constant) is expressed:

$$K_{ji} = \frac{\bar{a}_i}{a_i}\left(\frac{a_j}{\bar{a}_j}\right)^{z_i/z_j} \tag{A.1}$$

where K_{ji} is the equilibrium constant for i-component (BSA) to be adsorbed on the resin saturated with j-component (Cl^-). z_i is the ion valence for i-component, where $z_{BSA} = 4.9107$ and $z_{Cl^-} = 1$. a_i and $\bar{a}_i$ are the activities in the liquid and solid phases, respectively, defined as follows:

$$a_i = \gamma_i C_i, \quad i = \text{BSA or } Cl^- \tag{A.2}$$

$$\bar{a}_i = \bar{\gamma}_i z_i y_i, \quad i = \text{BSA or } Cl^- \tag{A.3}$$

where γ_i and $\bar{\gamma}_i$ are the liquid and surface activity coefficients, respectively, and y_i is the mol fraction in the solid phase:

$$y_i = \frac{n_i^*}{n_T}, \quad i = \text{BSA or } Cl^- \tag{A.4}$$

Note that (i) n_i^* has the units, (mmol/kg-resin), not (meq./kg-resin), and (ii) $n_{Cl^-}^*$ will not stoichiometrically be bound on the resin because the adsorbed salt counter-ions (Cl^-) may be sterically hindered by the macromolecule (BSA). The steric mass action is modeled as in Brooks and Cramer (1992):

$$n_T = z_{BSA} n_{BSA}^* + z_{Cl^-}\hat{n}_{Cl^-}^* + z_{Cl^-} n_{Cl^-}^* \tag{A.5}$$

where n_T is the resin capacity and $\hat{n}_{Cl^-}^*$ is the hindered salt concentration expressed as $\hat{n}_{Cl^-}^* = \sigma n_{BSA}^*$. As a result, Eq. (A.5) is:

$$n_T = n_{BSA}^*(z_{BSA} + \sigma) + n_{Cl^-}^* \tag{A.6}$$

where σ is the steric factor (or molar ratio of the hindered salt to proteins) which is set to $\sigma = 24.0$ for the BSA–NaCl

system. Thus, y_{Cl^-} means in Eq. (A.3) the molar fraction of Cl^- excluding the hindered salt ions ($\hat{n}^*_{Cl^-}$).

The liquid activity coefficient for BSA is assumed to be $\gamma_{BSA} = 1$ because protein solutions are in most cases dilute but γ_{NaCl} is defined by a Debye–Hückel model (Bromley, 1973):

$$\ln(\gamma_{NaCl}) = \frac{-0.511\sqrt{I}|z_+z_-|}{1+\sqrt{I}} + \frac{(0.06+0.6B)|z_+z_-|I}{(1+1.5I/|z_+z_-|)^2} + BI \quad (A.7)$$

where I is the ionic strength and the absolute value of the charge product, $|z_+z_-| = 1.0$, for the salt. The model constant B is known as $B = 0.0574$ for NaCl, which is assumed to be valid for the binary system (BSA–NaCl) because the protein concentration ($C_{BSA} = 0.9$ mmol/l) is much lower than that of the salt ($C_{NaCl} = 207$ mmol/l). Neglecting the protein effect on the salt activity, the salt ionic strength is expressed:

$$I = \frac{1}{2}\sum_{j=Na^+,Cl^-} m_j z_j^2 = m_{NaCl} \quad (A.8)$$

where m_i is the molarity (mol/kg-solvent). Here, the molarity is estimated on the basis of the molar concentration (C_i, mmol/l) for this dilute aqueous solution, assuming the solution density is 1.0 kg/l:

$$m_{NaCl} \approx \frac{1.0\times10^{-3}C_{NaCl}}{1-\sum_{j=BSA,NaCl}1.0\times10^{-6}C_jM_{wj}} \quad (A.9)$$

where the molecular weight (M_w) is $(M_w)_{BSA} \approx 69{,}000$ and $(M_w)_{NaCl} = 58.4$ g/mol.

In the isocratic mode, $\gamma_{NaCl} \approx 0.87$ at $C_{NaCl} = 0.207$ mol/l, which is quiet similar to experimental data for the pure NaCl solution at $I = 0.2$ in Bromley (1973).

The surface activity coefficient ($\bar{\gamma}_i$) is given in Raje and Pinto (1997):

$$\ln(\bar{\gamma}_i) = S_i\left[\ln\left(\sum_{j=1}^{2}\omega_j\alpha_{ji}\right) + 1 - \sum_{j=1}^{2}\frac{\omega_j\alpha_{ij}}{\sum_{k=1}^{2}\omega_k\alpha_{kj}}\right], \quad i = \text{BSA or } Cl^- \quad (A.10)$$

where S_i is the shape factor ($S_{BSA} = 13.55$ and $S_{Cl^-} = 1.0$), ω_i is the surface fraction and α_{ij} is the Boltzmann weighting factor. The surface fraction is defined:

$$\omega_i = \frac{S_iy_i}{\sum_{j=1}^{2}S_jy_j}, \quad i = \text{BSA or } Cl^- \quad (A.11)$$

The Boltzmann weighting factor is simply proposed for the BSA–NaCl system (Raje & Pinto, 1997):

$$\alpha_{Cl^-\text{–BSA}} = \exp\left(\frac{-mz_{BSA}y_{BSA}}{RT\times S_{BSA}}\right) \quad (A.12)$$

elsewhere $\alpha_{ij} = 1.0$. Here, $m = 18.0$ kcal/mol, $R = 1.9872\times10^{-3}$ kcal/(K mol) and $T = (35.4+273.15)$K. It is noted that the two model parameters (m and σ) are fit to the experimental data given in Li and Pinto (1995). In Fig. 7, experimental data and concentrations predicted by the model are shown with $m = 18.0$ and $\sigma = 24.0$. According to Raje and Pinto (1997), $K_{12} = 2.175\times10^{10}$ at $T = 35.4\,^\circ$C, in terms of the above units for the solid and liquid concentrations.

Finally, the equilibrium concentration functions, Eq. (A.1), are expressed as an implicit function of C_i and n_i^*, as shown in Eq. (1c):

$$g_i(C_{BSA}, C_{Cl^-}, n^*_{BSA}, n^*_{Cl^-}) = 0, \quad i = \text{BSA or } Cl^- \quad (A.13)$$

To solve Eq. (A.13), the Powell hybrid algorithm (from the IMSL numerical library) is used, where the relative tolerance of the variable differences (Δy_i) is set to 1.0×10^{-4} and the Jacobian is numerically evaluated.

References

Beste, Y. A., Lisso, M., Wozny, G., & Arlt, W. (2000). Optimization of simulated moving bed plants with low efficient stationary phases: Separation of fructose and glucose. *Journal of Chromatography A, 868*, 169–188.

Bromley, L. A. (1973). Thermodynamic properties of strong electrolytes in aqueous solutions. *AIChE Journal, 19*(2), 313–320.

Brooks, C. A., & Cramer, S. M. (1992). Steric mass-action ion exchange: Displacement profiles and induced salt gradients. *AIChE Journal, 38*(12), 1969–1978.

Chang, S. C. (1995). The method of space–time conservation element and solution element—A new approach for solving the Navier–Stokes and Euler equations. *Journal of Computers and Physics, 119*, 295–324.

Chang, S. C. (2002). Courant number insensitive CE/SE schemes. In *Proceedings of the 38th AIAA Joint Propulsion Conference*. AIAA-2002-3890, Indianapolis, USA.

Chang, S. C., & To, W. M. (1991). *A new numerical framework for solving conservation laws—The method of space–time conservation element and solution element*. NASA TM 104495.

Chang, S. C., Wang, X. Y., & Chow, C. Y. (1999). The space–time conservation element and solution element method: A new high-resolution and genuinely multidimensional paradigm for solving conservation laws. *Journal of Computers and Physics, 156*, 89.

Chang, S. C., Wang, X. Y., Chow, C. Y., & Himansu, A. (1995). *The method of space–time conservation element and solution element—Development of a new implicit solver*. NASA TM 106897.

Chang, S. C., Wang, X. Y., & To, W. M. (2000). Application of the space–time conservation element and solution element method to one-dimensional convection–diffusion problems. *Journal of Computers and Physics, 165*, 189–215.

Chang, S. C., Wu, Y., Wang, X. Y., & Yang, V. (2000). Local mesh refinement in the space–time CE/SE method. In *Proceeding of the First International Conference on CFD* (pp. 61–66). Kyoto, Japan.

Dunnebier, G., Weirich, I., & Klatt, K.-U. (1998). Computationally efficient dynamic modeling and simulation of simulated moving bed chromatographic processes with linear isotherms. *Chemical Engineering Science, 53*(14), 2537–2546.

Hindmarsch, A. C. (1980). LSODE and LSODI: Two new initial value ordinary differential equation solvers. *ACM SIGNUM Newsletter, 15*, 19–21.

Jiang, G., & Shu, C. W. (1996). Efficient implementation of weighted ENO schemes. *Journal of Computers and Physics, 126*, 202–228.

Li, Y., & Pinto, N. G. (1995). Model for ion-exchange equilibria of macromolecules in preparative chromatography. *Journal of Chromatography A, 702*, 113–123.

Lim, Y. I., Le Lann, J. M., & Joulia, X. (2001a). Accuracy, temporal performance and stability comparisons of discretization methods for the solution of Partial Differential Equations (PDEs) in the presence of steep moving fronts. *Computational Chemical Engineering, 25*, 1483–1492.

Lim, Y. I., Le Lann, J. M., & Joulia, X. (2001b). Moving mesh generation for tracking a shock or steep moving front. *Computational Chemical Engineering, 25*, 653–663.

Lim, Y. I., Le Lann, J. M., Meyer, X. M., Joulia, X., Lee, G. B., & Yoon, E. S. (2002). On the solution of Population Balance Equations (PBE) with accurate front tracking methods in practical crystallization processes. *Chemical Engineering Science, 57*, 177–194.

Ma, Z., & Wang, N.-H. L. (1997). Standing wave analysis of SMB chromatography: Linear systems. *AIChE Journal, 40*(10), 2488–2508.

Melis, S., Markos, J., Cao, G., & Morbidelli, M. (1996). Separation between amino acids and inorganic ions through ion exchange: Development of a lumped model. *Ind. Eng. Chem. Res., 35*, 3629–3636.

Molls, T., & Molls, F. (1998). Space–time conservation method applied to Saint Venant equations. *Journal of Hydraulic Engineering, 124*(5), 501–508.

Motz, S., Mitrovic, A., & Gilles, E.-D. (2002). Comparison of numerical methods for the simulation of dispersed phase systems. *Chemical Engineering Science, 57*, 4329–4344.

Pennington, S. V., & Berzins, M. (1993). *New NAG library software for first-other partial differential equations*. Research report series 93.21, University of Leeds, Leeds.

Petzold, L. R. (1983). In R. S. Stepleman, et al. (Eds.), *A description of DASSL: A differential/algebraic system solver in scientific computing* (pp. 65–68). North-Holland, Amsterdam.

Poulain, C. A., & Finlayson, B. A. (1993). A comparison of numerical methods applied to non-linear adsorption columns. *International Journal of Numerical Methods and Fluids, 17*(10), 839–859.

Raje, P., & Pinto, N. G. (1997). Combination of the steric mass action and non-ideal surface solution models for overload protein ion-exchange chromatography. *Journal of Chromatography A, 760*, 89–103.

Talu, O., & Zwiebel, I. (1986). Multicomponent adsorption equilibria of nonideal mixture. *AIChE Journal, 32*(8), 1263–1276.

Yu, S. T., & Chang, S. C. (1997). Treatment of stiff source terms in conservation laws by the method of space–time CE/SE, AIAA 97-0435, In *Proceedings of the 35th Aerospace Sciences Meeting*. Reno, USA.

Zhang, Z. C., Yu, S. T., & Chang, S. C. (2002). A space–time conservation element and solution element method for solving the two- and three-dimensional unsteady Euler equations using quadrilateral and hexahedral meshes. *Journal of Computers and Physics, 175*, 168–199.